Pattern-directed to isotropic dewetting transition in polymer films on micropatterned surfaces with differential surface energy contrast

Duangrut Julthongpiput, Wenhua Zhang, Jack F. Douglas, Alamgir Karim and Michael J. Fasolka*

Received 19th June 2006, Accepted 18th December 2006
First published as an Advance Article on the web 19th January 2007
DOI: 10.1039/b608630f

Surface chemical patterns can both cause and direct dewetting in overlying thin polymer films. In this paper we focus on a key factor in this phenomenon, the magnitude of the surface energy difference between surface pattern domains ($\Delta\gamma$). To probe the influence of $\Delta\gamma$ on film dewetting, we utilize novel combinatorial test patterns exhibiting a gradient in $\Delta\gamma$. Specifically, our test patterns consist of a series of micron-scale striped regions that continuously change in their surface energy (γ) relative to background striped regions having a fixed and calibrated γ. Using polystyrene (PS) films as a demonstration case, we employ these test patterns to quantify the morphology and kinetics of dewetting as $\Delta\gamma$ diminishes. Our study indicates a transition from pattern-directed to isotropic PS dewetting at critical $\Delta\gamma$ values. For $\Delta\gamma > 14$ mJ m^{-2}, ordered droplet arrays are formed, while for $\Delta\gamma < 7$ mJ m^{-2}, the dewetting is isotropic. A competition between these limiting behaviors is found for a ''crossover regime'', 7 mJ m^{-2} $< \Delta\gamma <$ 14 mJ m^{-2}. These combinatorial test patterns provide a powerful approach for investigating the large number of parameters that govern the stability of ultrathin polymer films, and the physical factors that influence the dewetted film morphology.

Introduction

Substrate heterogeneities can strongly influence the stability and the course of dewetting of supported thin films.[1–7] Scientific interest in this phenomenon is motivated, in part, by its practical importance. On the one hand, substrate chemical heterogeneities can drive film instabilities, and thus failure, in film applications such as barrier coatings, electronics packaging and resist systems. However, this same phenomenon has the potential for self-assembly based manufacturing since surface chemical patterns can ''direct'' dewetting morphology to create organized structures for a variety of applications.[8]

This paper examines the transition between the well studied case of isotropic film dewetting on chemically homogeneous substrates and the more recently investigated ''directed'' dewetting on chemically patterned substrates.[1,9–12] An earlier study[12] focused on the role of the geometrical dimensions of substrate chemical patterns in achieving an organization of droplet arrays. This previous work established the existence of lower and upper cutoff length scales above and below which the chemical patterns are effective in localizing droplet arrays on stripes, an effect which is also observed in simulations.[13] The present work focuses on how the magnitude of the *chemical contrast* $\Delta\gamma$, *i.e.* the surface energy differences between domains in a substrate pattern, affects the droplet morphology of a dewetted polymer film. While it is evident that the dewetting morphology must become isotropic in the limit of vanishing surface energy contrast, *i.e.* a homogeneous surface, there are only a few qualitative experimental observations[12] relating to how $\Delta\gamma$ influences the dewetting morphology. To address this important parameter systematically, we employ a combinatorial approach consisting of a gradient micropattern that exhibits a continuous change in chemical contrast. This test substrate allows a detailed and quantitative investigation of how pattern contrast influences the dewetting morphology on striped patterns and enables determination of a critical surface energy contrast for pattern-directed droplet organization.

Polymers Division, NIST, Gaithersburg MD 20899, USA. E-mail: mfasolka@nist.gov

Results and discussion

Fig. 1a schematically illustrates our gradient micropattern design. Fabrication of such substrates is discussed briefly below, and in detail elsewhere.[14,15] The crux of our combinatorial test surface is a series of micron-scale lines that continuously change in their surface energy (γ) with respect to a background matrix that exhibits constant γ. As noted below, these gradient micropatterns ($\nabla\mu p$) do not exhibit significant topography. The $\nabla\mu p$ pattern is bordered by two surface energy calibration fields that directly reflect γ in the gradient and matrix portions of the pattern. As an essential part of the library design, we perform contact angle measurements along each of the calibration fields to determine the local $\Delta\gamma$ along the $\nabla\mu p$.[15] Our $\nabla\mu p$ test pattern consisted of 20 μm-wide *n*-octyldimethylchlorosilane (ODS) self-assembled monolayer (SAM) domains separated by 4 μm lines of a SiO_2 reference matrix. The surface energy on the hydrophilic matrix field (γ_{SiO2}) was measured to be $\approx$67 mJ m^{-2}. The surface energy of the $\nabla\mu p$ lines and calibration gradient field was modulated through a graded UV-ozonolysis (UVO) of the ODS SAM. Based on water contact angle measurements along the gradient calibration field, the surface energy of the lines (γ_{SAM}) spanned a range of 20 mJ m^{-2} to 63 mJ m^{-2}. Based on these

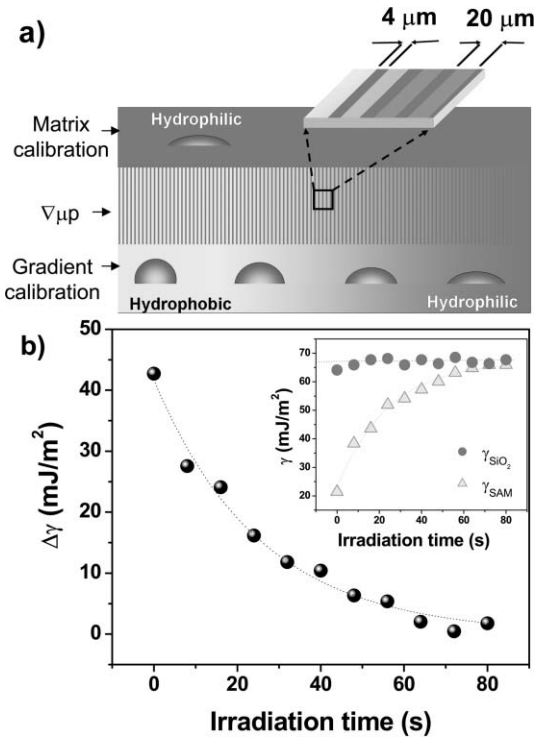

Fig. 1 (Top) Schematic illustration of gradient test specimen design. (Bottom) Surface energy contrast, $\Delta\gamma \equiv \gamma_{SiO2} - \gamma_{SAM}$, along the gradient micropattern. The inset shows surface energies along matrix (γ_{SiO2}) and gradient (γ_{SAM}) calibration fields. Error bars represent one standard deviation of the data, which is taken as the experimental uncertainty of the measurement. Lines are added to guide the eye.

measurements, the γ-contrast ($\Delta\gamma \equiv \gamma_{SiO2} - \gamma_{SAM}$) along the $\nabla\mu p$ decreased from 44 mJ m^{-2} to 3 mJ m^{-2}, as shown in Fig. 1b. As measured by atomic force microscopy, height differences between the SAM and SiO_2 domains were $\leqslant 1$ nm.

In this paper, we employ $\nabla\mu p$ test substrates to investigate the dewetted film morphology of thin polystyrene (PS) films on chemically heterogeneous surfaces. A 35 nm thick PS film (molecular mass 760 g mol^{-1}) was deposited on the $\nabla\mu p$ substrate and the film was annealed at 60° C until the dewetting was complete—approximately 12 h. We emphasize that the γ-gradients involved in our measurements are shallow, with a slope of approximately 1 mJ m^{-2} mm^{-1}, so the surface energy on each stripe of the micropattern and across sub-millimetre portions of the gradient SAM are effectively *constant*. Accordingly, the gradient will not cause long range movements of the relatively high viscosity polymer fluid along the specimen—all of the phenomena we discuss below is due to "local" surface conditions, and notably the surface energy is constant along the stripe (orthogonal to UVO gradient) direction. Moreover, we do not consider here the very long time regime, considered previously by Sehgal *et al.*,[12] where random droplet motion can lead to coalesced droplets that span adjacent stripes.

Fig. 2 shows a comprehensive library of the dewetted PS film morphology, compiled using an automated optical microscopy (OM) system,[17] which acquired and collated 1900 contiguous micrographs spanning the entire specimen. A schematic of the gradient test specimen indicates the orientation of the stripe patterns, while the bottom of Fig. 2 shows four magnified strips of OM data extracted from the library. The top and bottom sections of each stripe region show OM data from the unpatterned matrix calibration region (SiO_2) and the gradient calibration region (UVO-modified ODS SAM), respectively. The middle section of each data strip shows the transition from pattern-directed to isotropic dewetting over the $\nabla\mu p$ and includes highlight images that detail representative film morphologies.

Along the unpatterned matrix and gradient calibration fields, the film exhibits the well known polygonal droplet patterns characteristic of dewetted films exhibiting a random nucleation of isotropic holes. This is the reference case for our comparisons to pattern-directed dewetting below. Previous studies indicate that isotropic dewetting occurs in four stages.[18,19] In the early stage, holes are generated by a film rupture process. In the intermediate stage, the radii of the holes increase. In the third stage, the holes impinge to create a froth-like network[20] whose thread-like boundaries break into droplets in the final stage by a process that resembles a Rayleigh instability.[7,21] This dewetting process is distinct from spinodal dewetting in ultrathin films where a rather uniform distribution of droplets forms due to capillary instabilities.[12,22] Because of the unchanging γ in this region, the matrix calibration field exhibits a similar final droplet morphology along the specimen, as illustrated through the top of strips (a)–(d) in Fig. 2. In contrast, as γ increases from strip (a) to (d) on the gradient calibration field (bottom), the droplets become increasingly large, and are arranged in larger polygonal patterns. In this system, the scale of the polygonal patterns is likely determined by the rate of hole nucleation, which increases as γ increases, rather than the rate of hole growth, which is expected to be slow and constant based on observations of ultrathin PS films deposited on substrates having a similar range of γ.[23] These issues will be discussed further below

The morphology of droplets formed over the $\nabla\mu p$ pattern varies as the $\Delta\gamma$ of the pattern decreases from strip (a) to strip (d). A cursory analysis of the micrographs immediately indicates three regions of dewetted droplet morphology, denoted as I, II and III throughout the rest of the paper (see Fig. 2). In Region I (high $\Delta\gamma$), we observe a *pattern-directed* morphology similar to that reported by Sehgal *et al.*[12] and Luo *et al.*[10] Region I is characterized by arrays of droplets distributed along the center of both the matrix and SAM portions of the pattern. In Region II, we observed a *cross over* behavior where the droplets gradually lose registry with the underlying pattern as $\Delta\gamma$ becomes weaker (Fig. 2b and 2c). Finally, in Region III, we observe *isotropic dewetting*, characterized by droplet polygons of the same dimensions seen in each of the adjacent calibration fields (Fig. 2d).

A more detailed picture of the dewetting behavior is obtained through automated image analysis of the late stage film morphology, and through real time optical microscopy observations of the morphology development at representative points along the patterned area. The results of this image analysis are presented in Fig. 3, which presents histogram distributions of final PS droplet diameters as $\Delta\gamma$ decreases along the specimen. Our data are summarized in Fig. 4, which plots the number density of droplets over SiO_2 and SAM

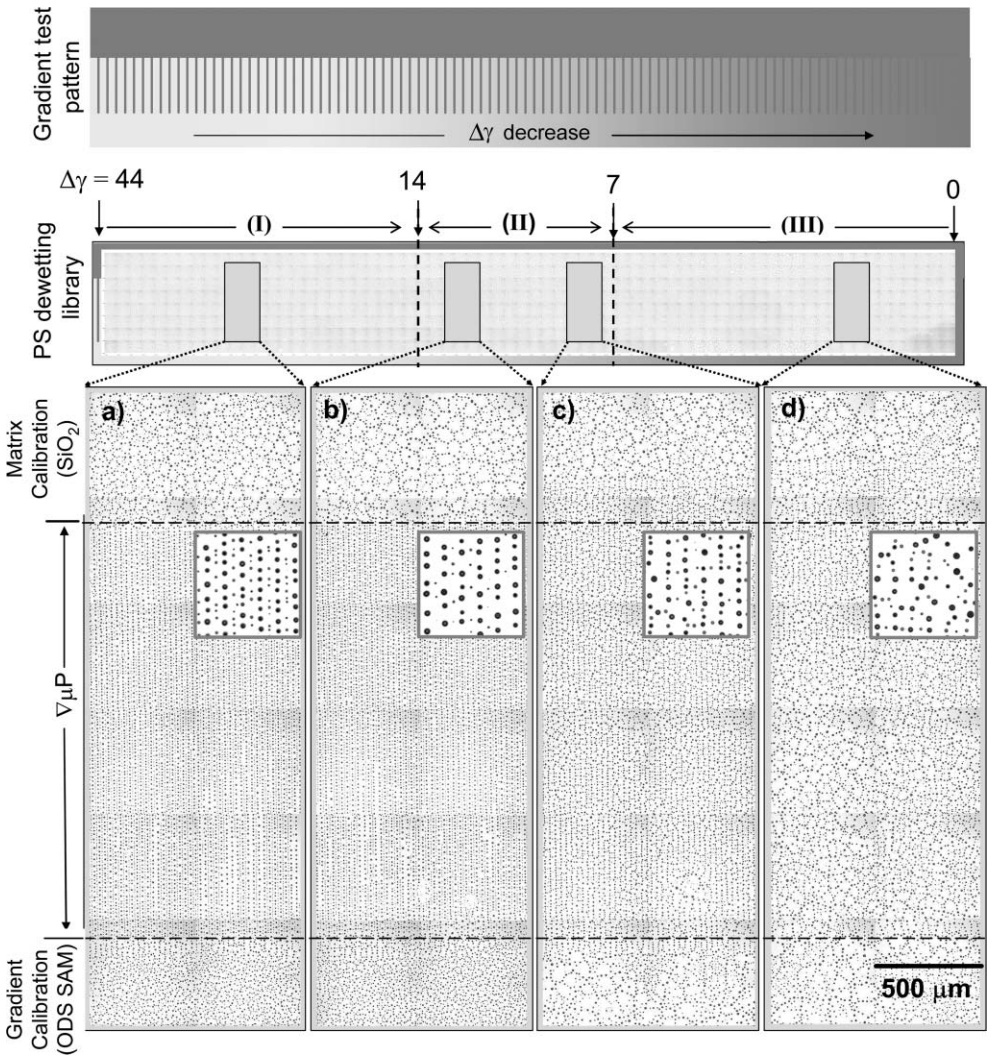

Fig. 2 (Top) Schematic of the gradient test pattern illustrating pattern and gradient orientation in the experiments. (Middle) PS dewetting library compiled from 1900 contiguous optical micrographs over the entire specimen. Regions I, II and III, noted on the figure, are discussed in the text. (a–d) Strips of OM data extracted from the library showing the transition from pattern-directed to isotropic dewetting. Insets (250 μm × 250 μm) show magnified OM micrographs of representative dewetting morphologies.

domains versus $\Delta\gamma$ and γ_{SAM}. The droplet size distribution data (Fig. 3) reveals several key observations. For $\Delta\gamma$ values between 44 mJ m^{-2} and 7 mJ m^{-2} (Regions I and II), the droplets exhibit a bimodal size distribution characteristic of pattern-directed dewetting.[12] Over this range, the droplet diameters remain relatively constant, which suggests that the width of the chemical stripes largely regulates the ultimate droplet size on that domain. However, as indicated in Fig. 4, the number density of smaller PS droplets over the SiO_2 pattern domains changes dramatically as a function of $\Delta\gamma$, which suggests directed and differential fluid flow between the stripe domains in the early stage of the film dewetting process. Observations of surface energy driven transport on patterned surfaces have also been made by Lee and Laibinis.[16] These authors demonstrated that differences in the dynamic contact angle between the leading and trailing ends of a droplet caused long-range (mm-scale) movement along a narrow stripe imparted with a steep γ-gradient. Our case differs from the work of Lee and Laibinis because the fluid motion occurs *transverse* to the stripe axis. We return to this phenomenon in our discussion below.

For $\Delta\gamma < 7$ mJ m^{-2} (Region III), we observe a broad monomodal distribution of droplets indicative of isotropic dewetting. From this analysis, we can immediately identify the range of $\Delta\gamma$ for well patterned droplets, *i.e.* between 14 mJ m^{-2} and 25 mJ m^{-2}, and a critical $\Delta\gamma$ necessary to induce pattern-directed dewetting, $\Delta\gamma_c \approx 7$ mJ m^{-2}. Moreover, our image data and real time OM observations suggest a dewetting mechanism for each of these three regions.

In Region I, where $\Delta\gamma$ is high, dewetting occurs in two steps. First, the large $\Delta\gamma$ between the domains drives a rapid localization of the PS liquid into long threads centered over the pattern stripes. Next, similar to the final stage of isotropic dewetting described above, the localized threads rupture *via* a capillary instability to form lines of droplets. This process was too fast to be captured by our automated OM measurements, but real time OM observations indicate that thread break-up occurs through a rapid, collective disintegration, *i.e.* droplets

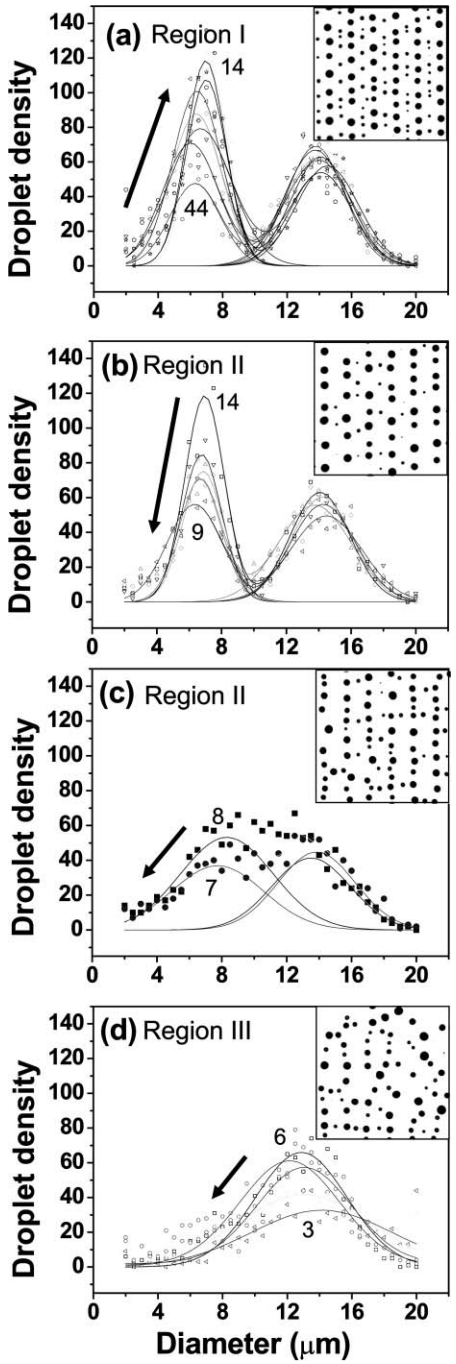

Fig. 3 Histograms of PS droplet size distribution for dewetting Regions I–III. *Droplet density* is taken as the number of droplets of a given size in a 0.5 mm × 0.5 mm optical micrograph. (a) Region I: $\Delta\gamma$ is 44 mJ m^{-2} to 14 mJ m^{-2}; (b–c) Region II: $\Delta\gamma$ is 13 mJ m^{-2} to 9 mJ m^{-2} and 8 mJ m^{-2} to 7 mJ m^{-2} respectively; (d) Region III: $\Delta\gamma$ is 6 mJ m^{-2} to 3 mJ m^{-2}. Symbols distinguish individual data sets. Arrows indicate histogram progression as $\Delta\gamma$ decreases. Lines show Gaussian fits to histogram data.

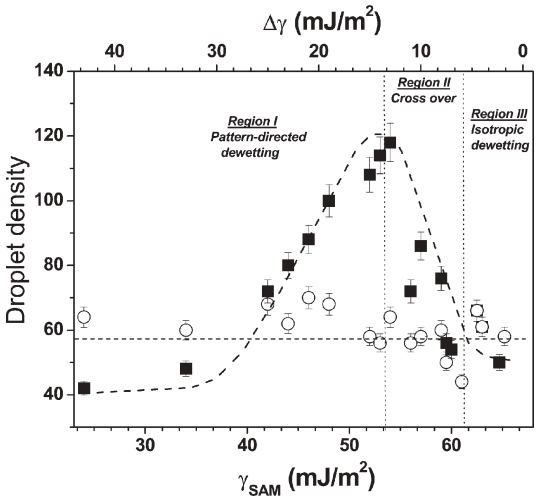

Fig. 4 Summary of droplet density measurements, extracted from histograms in Fig. 3, versus $\Delta\gamma$ over the range of 3 mJ m^{-2} to 44 mJ m^{-2}. (■) denotes data for droplets over SiO_2 domains; (○) denotes data for droplets over SAM domains. Error bars represent one standard deviation of the data, which is taken as the experimental uncertainty of the measurement. Lines are added to guide the eye.

are formed "all at once" from the thread. As posited in previous treatments[4], surface supported thread patterns should not disintegrate due to polymer–air interactions alone since the surrounding air has a relatively low viscosity. Accordingly, we hypothesize that thread break-up corresponds to a hybrid form of capillary instability that combines dewetting and interfacial energy driven effects, and that has not been previously investigated either experimentally or theoretically. This sort of capillary instability, coupled with the reasonable expectation that the thread width is governed by the stripe width and γ, accounts for the highly regular size and spacing of the droplets in these arrays. As evidenced by the final droplet densities over each stripe (Fig. 4), formation of the PS threads apparently involves a concurrent short-range redistribution of fluid from lower γ SAM stripes to the higher surface energy SiO_2 domains. For $\Delta\gamma > 29$ mJ m^{-2}, which corresponds to conditions where $\gamma_{SAM} \geqslant \gamma_{PS}$, transfer of the PS liquid is relatively weak, even though the kinetics of the break-up process are fast, as described below. For $\Delta\gamma$ values below 29 mJ m^{-2}, the transfer of fluid to the higher-γ SiO_2 stripes increases until $\Delta\gamma \approx 14$ mJ m^{-2}, which marks the onset of Region II.

The dewetting process is more complicated in Region II and seems to reflect a *competition* between the pattern-directed and isotropic dewetting processes. As opposed to the formation of well defined fluid threads that are characteristic of Region I, the dewetting in this regime proceeds through the formation and growth of holes similar to the case of unpatterned substrates. However, after they form, these holes become elongated along the axis of the stripes and then grow rapidly in this direction while growing relatively slowly in the direction perpendicular to the pattern. The fast-growing edges of these elongated holes exhibit a series of tendrils that extend a short distance from the receding dewetting front before 'pinching off' to form lines of droplets that are localized over the pattern domains. This droplet formation from the dewetting front resembles dewetting systems that exhibit competing instabilities such as in solution cast polymer films where dewetting is accompanied by simultaneous solvent evaporation,[24] or in fluids that exhibit simultaneous dewetting and phase separation.[25] As $\Delta\gamma$ decreases from 14 mJ m^{-2} to 7 mJ m^{-2}, the holes

become more isotropic. In addition, the density of droplets sequestered over the SiO_2 domains decreases, which suggests that fluid flow towards these domains become reduced as $\Delta\gamma$ diminishes. Finally, when $\Delta\gamma$ drops below 7 mJ m^{-2} (Region III), we observed isotropic hole growth and broad droplet size distributions characteristic of the isotropic dewetting seen in the adjacent unpatterned calibration areas. In this regime, $\Delta\gamma$ is too weak to drive fluid redistribution between the pattern domains and dewetting is like that on a homogeneous surface.

To examine these phenomena further, we measured the kinetics of dewetting along the specimen, concentrating on the transitions from Regions I to II, and from Regions II to III. Fig. 5 shows representative OM images of film ruptures over both the non-patterned (a) and ∇μp (b) regions of the substrate. Along the ∇μp, the largest dimensions of anisotropic holes parallel (R_y) and perpendicular (R_x) to the pattern domains were measured over time, yielding the respective hole growth velocities $V_y = dR_y/dt$ and $V_x = dR_x/dt$ along these directions. For comparison, the growth velocities of isotropic holes were measured on the matrix (V_{SiO2}) and SAM calibration fields (V_{SAM}). Fig. 5c plots a summary of the hole growth velocities as a function of $\Delta\gamma$ and γ_{SAM}.. We observed nearly constant hole growth rates, $V_{SiO2} \approx 2$ μm s^{-1}, along the matrix calibration field. Over most of the SAM calibration field, we found V_{SAM} to be very small and nearly invariant

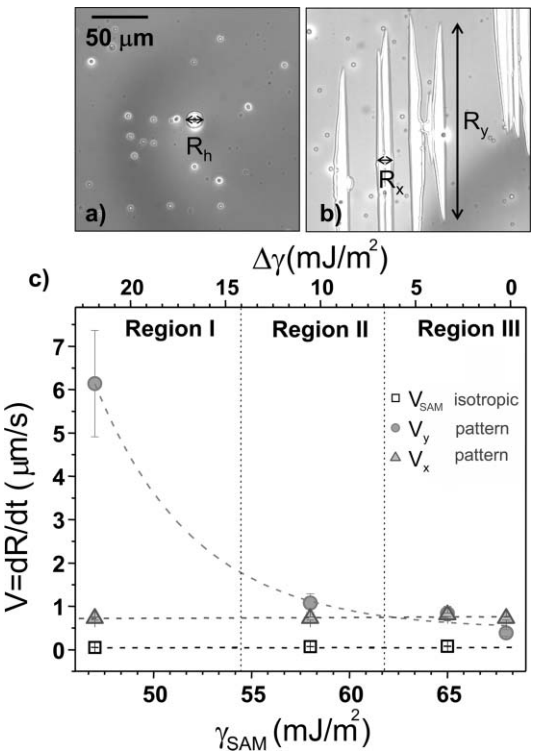

Fig. 5 Dewetting kinetics. OM images of dewetting holes of PS film on (a) non-patterned SAM gradient calibration field and (b) ∇μp during annealing at 60 °C at comparable times. (c) Dewetting hole growth velocity ($V = dR/dt$) *vs.* $\Delta\gamma$ and γ_{SAM}. V_y and V_x are the rate of the pattern-directed dewetting on the ∇μp measured parallel and perpendicular to the pattern stripes respectively. V_{SAM} is the isotropic hole growth velocity over the gradient SAM calibration field. Error bars represent one standard deviation of the data, which is taken as the experimental uncertainty of the measurement. Lines are added to guide the eye.

with respect to γ_{SAM}. This is consistent with previous findings of Ashley *et al.*,[23] who observed PS films of similar thickness and molecular mass to be marginally stable over a similar range of substrate γ. At the high-γ extreme of the SAM gradient, where γ was measured to be ≈68 mJ m^{-2}, V_{SAM} was observed to abruptly approach V_{SiO2}. This is likely due to the fact that prolonged UVO exposure will eventually consume the SAM layer and reduce the surface to bare SiO_2.[26] While it might be expected that polymer films would be stable on these higher-γ SiO_2/Si substrates, our cleaning procedure imparts a residual oxide layer with highly polar moieties that are not necessarily homogeneously distributed.[23] For these reasons, we do not include this data point (γ_{SAM} = 68.5 mJ m^{-2}) in Fig. 5.

The monotonic increase of V_y with $\Delta\gamma$ along the ∇μp is perhaps the most conspicuous feature of Fig. 5. This trend is qualitatively consistent with the simulations of Sharma and coworkers,[22,27] which indicate that a large $\Delta\gamma$ can drive dewetting even when the individual surfaces constituent to the pattern are expected to exhibit stable films. While we do not provide a quantitative explanation for the dependance of V_y on $\Delta\gamma$ in Fig. 5c, this behavior is qualitatively rooted in the local surface energy gradients normal to the stripe direction, which induce fluid flow from the less wettable to more wettable substrate regions.[16,22,27] Indeed, this local redistribution of polymer is directly reflected in the droplet distribution data we present in Fig. 3 and Fig. 4.

Along the ∇μp, the observed kinetics correlate with the regions of dewetting behavior defined above. At the edge of Region I shown in Fig. 5c, we have $V_y >> V_x$, indicating pattern-directed dewetting. Here, the large V_y is driven by the infinite three-phase contact line along which $\Delta\gamma$ is large. In contrast, V_x is hampered by the interleaved pattern of SAM and SiO_2 regions, both of which exhibit the relatively slow hole growth rates (V_{SAM} and V_{SiO2}) we measured along the calibration fields. Accordingly, the border between Regions I and II is seemingly marked by the point at which V_y falls below the barrier value of V_{SiO2}. In this crossover regime, anisotropic hole growth still occurs, *i.e.*, $V_y > V_x$. However, V_y approaches V_x over this range of $\Delta\gamma$, indicating a competition between pattern-directed and isotropic dewetting processes. Finally, in Region III, V_y approaches V_{SAM}, and $V_y \approx V_x$, indicative of isotropic dewetting.

Note added in proof

While our paper was in press, we became aware of a recent article[28] that describes the capillary instability of film 'threads' on unpatterned substrates. Our observation of thread break-up on chemically striped regions is consistent with the theory and data presented in this recent work.

Experimental†

Our fabrication of ∇μp specimens involves soft-lithography of ODS (Gelest, Inc) SAM molecules onto a planar substrate

† Equipment and instruments or materials are identified in the paper in order to adequately specify the experimental details. Such identification does not imply recommendation by NIST, nor does it imply the materials are necessarily the best available for the purpose.

followed by a graded processing step that modulates the chemical contrast.[15] A gradient test specimen is prepared by conditioning the patterned ODS SAM with a graded UVO treatment. Under UVO treatment, a range of oxygen-containing functionalities are added to the ODS molecules, including carboxylate, ether and carbonyl species.[26] For our specimens, the surface energy (γ) was estimated by the Good and Girifalco geometric mean approximation method,[29] which employs contact angle measurements of two fluids for which the polar and the dispersive components of γ are known. The procedure for estimating γ for UVO-modified ODS surfaces is discussed in detail elsewhere.[26] Atomic Force Microscopy (D3100, Digital Instruments) was used to measure height differences between the SAM and SiO_2 domains. Dewetting experiments involved PS (nominal molecular mass = 760 g mol^{-1}, Cat No. 32782-4, Aldrich) films spin-coated from toluene solutions (mass fraction of 1%) onto a fresh $\nabla\mu$p specimen. The as-cast film was smooth and uniform as determined by immediate optical inspection, and measured to be 35 nm $\pm$ 1 nm across the entire specimen *via* variable angle spectroscopic ellipsometry (J.A. Woolam Inc.). The system was annealed at 60 °C for at least 12 h to accelerate dewetting; the glass transition temperature of PS at this relative molecular mass is approximately 45 °C.[12] Automated OM measurements[17] were conducted using a microscope (Nikon Optiphot II) fitted with a motorized *x*–*y* stage (Ludl) and digital camera (Hitachi VK-C350), and driven by custom software (Python Software Foundation). Automated image processing was accomplished through custom routines (IDL, ITT Industries Inc.). Droplet size data were drawn from OM micrographs having the dimensions, 0.5 mm $\times$ 0.5 mm.

Conclusions

In conclusion, we stress the advantages of our experimental approach, specifically the use of gradient combinatorial test substrates, which provided a unique, powerful platform for examining the dewetting behavior of films. Since the $\nabla\mu$p exhibited a comprehensive, systematic and calibrated variation in pattern chemical contrast ($\Delta\gamma$), we were able to thoroughly and quantitatively examine the effect of this under-evaluated variable on the system behavior. Our study demonstrates that surface energy contrast, $\Delta\gamma$, is a parameter that dictates whether polymer films undergo pattern-directed or isotropic dewetting. Three regimes of dewetting behavior, encompassing the crossover between pattern directed and isotropic dewetting, were observed for high, intermediate and low $\Delta\gamma$ ranges. Moreover, we demonstrate that substrate patterns require a critical magnitude of $\Delta\gamma$ to be effective in creating ordered droplet arrays. Our observations also suggest a new type of capillary instability which is driven by fluid–solid substrate interactions rather than fluid–air interactions. While our study involved a particular polymer, it is evident that this experimental scheme could be extended easily to other dewetting systems, and towards the study of other film and surface phenomena, including self-assembly, adsorption and cell behavior.

Acknowledgements

The authors thank the NIST MSEL Director's Reserve Program and the NIST Advanced Technology Program for funding. Thanks to Kimberly Briggman and Thomas Germer (Optical Technology Division, NIST) for assistance with ellipsometry and for help in preparing lithographic masks respectively. This work made use of facilities at the NIST Combinatorial Methods Center. This work is an official contribution of the National Institute of Standards and Technology; not subject to copyright in the United States.

References

1 A. Checco, O. Gang and B. M. Ocko, *Phys. Rev. Lett.*, 2006, **96**, 056104.
2 S. Dietrich, M. N. Popescu and M. Rauscher, *J. Phys.: Condens. Matter*, 2005, **17**, S577–S593.
3 O. Gang, K. J. Alvine, M. Fukuto, P. S. Pershan, C. T. Black and B. M. Ocko, *Phys. Rev. Lett.*, 2005, **95**, 217801.
4 H. Gau, S. Herminghaus, P. Lenz and R. Lipowsky, *Science*, 1999, **283**, 46–49.
5 M. Geoghegan, C. Wang, N. Rehse, R. Magerle and G. Krausch, *J. Phys.: Condens. Matter*, 2005, **17**, S389–S402.
6 R. Lipowsky, M. Brinkmann, R. Dimova, T. Franke, J. Kierfeld and X. Z. Zhang, *J. Phys.: Condens. Matter*, 2005, **17**, S537–S558.
7 G. Nisato, B. D. Ermi, J. F. Douglas and A. Karim, *Macromolecules*, 1999, **32**, 2356–2364.
8 A. M. Higgins and R. A. L. Jones, *Nature*, 2000, **404**, 476–478.
9 P. Damman, N. Baudelet and G. Reiter, *Phys. Rev. Lett.*, 2003, **91**, 216101.
10 C. X. Luo, R. B. Xing, Z. X. Zhang, J. Fu and Y. C. Han, *J. Colloid Interface Sci.*, 2004, **269**, 158–163.
11 G. Reiter, *Langmuir*, 1993, **9**, 1344–1351.
12 A. Sehgal, V. Ferreiro, J. F. Douglas, E. J. Amis and A. Karim, *Langmuir*, 2002, **18**, 7041–7048.
13 K. Kargupta and A. Sharma, *Phys. Rev. Lett.*, 2001, **86**, 4536–4539.
14 D. Julthongpiput, M. J. Fasolka and E. J. Amis, *Microsc. Today*, 2004, **12**, 48–51.
15 D. Julthongpiput, M. J. Fasolka, W. H. Zhang, T. Nguyen and E. J. Amis, *Nano Lett.*, 2005, **5**, 1535–1540.
16 S. W. Lee and P. E. Laibinis, *J. Am. Chem. Soc.*, 2000, **122**, 5395–5396.
17 S.-W. Kim, A. Sehgal, A. Karim and M. J. Fasolka, *Microsc. Today*, 2003, **11**, 30–32.
18 K. M. Ashley, J. C. Meredith, E. J. Amis, D. Raghavan and A. Karim, *Polymer*, 2003, **44**, 769–772.
19 R. Xie, A. Karim, J. F. Douglas, C. C. Han and R. A. Weiss, *Phys. Rev. Lett.*, 1998, **81**, 1251–1254.
20 K. A. Barnes, J. F. Douglas, D. W. Liu and A. Karim, *Adv. Colloid Interface Sci.*, 2001, **94**, 83–104.
21 R. Seemann, S. Herminghaus, C. Neto, S. Schlagowski, D. Podzimek, R. Konrad, H. Mantz and K. Jacobs, *J. Phys.: Condens. Matter*, 2005, **17**, S267–S290.
22 R. Konnur, K. Kargupta and A. Sharma, *Phys. Rev. Lett.*, 2000, **84**, 931–934.
23 K. M. Ashley, D. Raghavan, J. F. Douglas and A. Karim, *Langmuir*, 2005, **21**, 9518–9523.
24 O. Karthaus, L. Grasjo, N. Maruyama and M. Shimomura, *Chaos*, 1999, **9**, 308–314.
25 R. Yerushalmi-Rozen, T. Kerle and J. Klein, *Science*, 1999, **285**, 1254–1256.
26 S. V. Roberson, A. J. Fahey, A. Sehgal and A. Karim, *Appl. Surf. Sci.*, 2002, **200**, 150–164.
27 M. Zope, K. Kargupta and A. Sharma, *J. Chem. Phys.*, 2001, **114**, 7211–7221.
28 J.-Y. Park, K. Y. Suh, S.-M. Soo and H. H. Lee, *J. Chem. Phys.*, 2006, **124**, 214710.
29 R. J. Good and L. A. Girifalco, *J. Phys. Chem.*, 1960, **64**, 561.